PERGAMON

International Journal of Rock Mechanics & Mining Sciences 40 (2003) 41–53

International Journal of
Rock Mechanics
and Mining Sciences

www.elsevier.com/locate/ijrmms

A constitutive model for rock interfaces and joints

J.G. Wang[a,*], Y. Ichikawa[b], C.F. Leung[c]

[a] *Tropical Marine Science Institute, National University of Singapore, 10 Kent Ridge Crescent, Singapore 119260, Singapore*
[b] *Division of Environmental Engineering and Architecture, Graduate School of Environmental Studies, Nagoya University, Nagoya 464-8603, Japan*
[c] *Department of Civil Engineering, National University of Singapore, 1 Engineering Drive 2, Singapore 117576, Singapore*

Accepted 15 September 2002

Abstract

A constitutive model based on limit concept is proposed to predict the behavior of rock interfaces and joints. For the limit case of an interface with thickness approaching zero, an ellipse yield function is adopted and associated flow rule is recommended. This yield function is not of proportional type, and its motion in stress space is governed by its center position and the hardening rule of yield function. The shear anisotropy is described by a shape function that incorporates the elastic shear stiffness, yield function and hardening rule. An equivalent relative displacement is obtained based on normalized plastic work and limit concept. This equivalent relative displacement yields a hardening rule from which the dilatancy is directly associated with the asperity of the interface. The validity of the proposed constitutive model is verified using data obtained from several existing experimental studies on natural and artificial rock joints.

1. Introduction

The behavior of rock mass is strongly affected by the presence of discontinuities such as joints, fissures, and faults. It has been widely reported that the deformation behavior of rock joint or interface is complicated even under simple deformation paths [1–4]. Several constitutive models have been proposed to predict the mechanical behavior of rock interface. These models, for example, include the hyperbolic model [5]; elastic–perfectly plastic model with Mohr–Coulomb friction law; modified Ramberg–Osgood-type model; directional-dependent model; and the HISS model [2,6]. Using the disturbed state concept, the HISS model regards an interface being made up of two materials: intact rock with plastic deformation and damaged rock with sliding. The deformation of the interface is contributed by both the intact rock and the damaged rock. Although the above models can successfully predict the shear deformation of an interface to a certain extent, the following issues have not been fully resolved. (1) The normal responses of an interface have not been properly considered in most of the models except the HISS model [2] and the Jing's model [4]. (2) The basic concepts of plasticity such as yield function, flow rule and hardening rule are widely used in the constitutive laws of interfaces, although these concepts were originally proposed for a solid instead of an interface. The fundamental theory for the transplantation from a solid to an interface has not been clearly established. (3) Non-associated flow is strongly recommended for elasto-plastic constitutive models of rock joints. Although non-associated flow rule is appropriate to describe the dilatancy and plastic deformation of the interface, the use of such flow rule often results in numerical difficulties such as instability and non-symmetry in the global stiffness. On the other hand, the use of associated flow rule does not usually experience numerical problems. Is it possible to adopt associated flow rule to describe the behavior of an interface while other properties of non-associated flow rule remain?

Although joints, fissures or faults occupy space and have thickness as shown in Fig. 1, the magnitude of thickness is much smaller than the other dimensions of the rock mass. Different modeling methods have been employed by various researchers. An interface can be treated as a thin layer problem [7], or a zero-thickness problem [8,16]. From the physical point of view, both

*Corresponding author. Tel.: +65-6874-6591; fax: +65-6779-1635.
E-mail address: tmswjg@nus.edu.sg (J.G. Wang).

1365-1609/02/$ - see front matter
PII: S1365-1609(02)00113-2

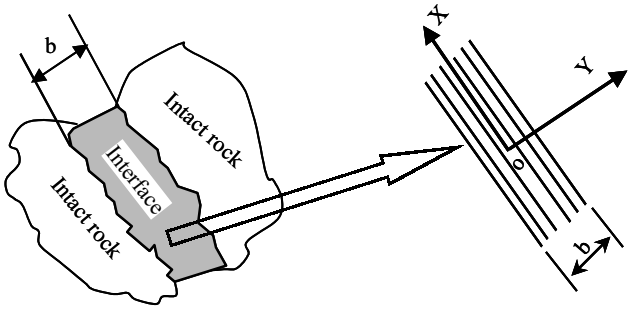

Fig. 1. Local coordinates for an interface with finite thickness.

simplifications are essentially the same because the thin layer model includes zero-thickness model as a special case [9]. However, the mathematical treatments and numerical performance may be different for different simplifications. In the present study, a constitutive law of interfaces based on the limit concept is proposed. For the limit case of an interface having thickness approaching zero, a particular form of yield function is recommended. The proposed constitutive model is different from the other constitutive models in four aspects. (1) Yield surface is not a proportional ellipse. The motion of the yield function in stress space is controlled by its center position and hardening rule. Both factors are independent of each other. (2) A shape function is introduced into the yield function and hardening rule to consider shear anisotropy. (3) A hardening rule is derived based on normalized plastic work. (4) Associated flow rule is recommended. This paper is organized as follows: Section 2 presents the limit concept and develops a constitutive law for an interface and Section 3 presents the material parameters. Section 4 compares the numerical simulations with three sets of experimental data. The limitations for the present constitutive model are also discussed in this paper.

2. Limit concept and constitutive law of an interface

The sign convention adopted in the present study is that compressive stress and deformation are positive. The elastic/recoverable deformation or strain is denoted by superscript "e" and the plastic/irreversible deformation or strain is denoted by superscript "p".

2.1. Constitutive relation of an interface with finite thickness

Fig. 1 shows a sketch of an interface between two intact rocks with a finite thickness b. The strain increment, $\mathrm{d}\boldsymbol{\varepsilon}$, of the interface can be divided into its elastic component, $\mathrm{d}\boldsymbol{\varepsilon}^{\mathrm{e}}$, and its plastic component, $\mathrm{d}\boldsymbol{\varepsilon}^{\mathrm{p}}$:

$$\mathrm{d}\boldsymbol{\varepsilon} = \mathrm{d}\boldsymbol{\varepsilon}^{\mathrm{e}} + \mathrm{d}\boldsymbol{\varepsilon}^{\mathrm{p}}. \tag{1}$$

The elastic component follows the incremental Hooke's law such that

$$\{\mathrm{d}\boldsymbol{\sigma}\} = [D]^{\mathrm{e}}\,\{\mathrm{d}\boldsymbol{\varepsilon}^{\mathrm{e}}\}, \tag{2}$$

where σ is stress tensor (the components are σ_{ij}) and $[D]^{\mathrm{e}}$ is the elastic matrix of materials.

The plastic component can be described using the plastic potential theory of plasticity as

$$\mathrm{d}\varepsilon_{ij}^{\mathrm{p}} = \mathrm{d}\lambda\frac{\partial g}{\partial \sigma_{ij}}, \tag{3}$$

where $\mathrm{d}\lambda$ is the plastic flow factor and g is the plastic potential function.

A consistency condition of deformation can be expressed as

$$\left\{\frac{\partial f}{\partial \boldsymbol{\sigma}}\right\}^{\mathrm{T}}\{\mathrm{d}\boldsymbol{\sigma}\} + \frac{\partial f}{\partial H}\mathrm{d}H = 0, \tag{4}$$

where f is a yield function with hardening rule H and superscript "T" refers to the transpose of a matrix. The generalized plastic derivatoric strain, $\varepsilon'^{\mathrm{p}}$, is expressed as $\varepsilon'^{\mathrm{p}}(=\sqrt{(2/3)\varepsilon'^{\mathrm{p}}_{ij}\varepsilon'^{\mathrm{p}}_{ij}})$ where $\varepsilon'^{\mathrm{p}}_{ij} = \varepsilon^{\mathrm{p}}_{ij} - \bar{\varepsilon}^{\mathrm{p}}\delta_{ij}$, $\bar{\varepsilon}^{\mathrm{p}}(=(1/3)\varepsilon^{\mathrm{p}}_{ii})$ and δ_{ij} is Kronecker delta. For convenience a local coordinate $(x-y)$ system is adopted in the present analysis, as shown in Fig. 1. Sharma and Desai [9] reported that it is reasonable to assume the normal stress σ_x along thickness or x-direction has little effect on the plastic potential, $g = g(\sigma_y, \tau_{xy}, H)$ where σ_y is the normal stress and τ_{xy} is the shear stress. The hardening rule H is assumed to be $H = H(\bar{\varepsilon}^{\mathrm{p}}, \varepsilon'^{\mathrm{p}})$. The plastic modulus, A^*, is defined as

$$A^*\,\mathrm{d}\lambda = -\frac{\partial f}{\partial H}\mathrm{d}H. \tag{5}$$

For an interface, this leads to

$$A^* = -\frac{\partial f}{\partial H}\left(\frac{\partial g}{\partial \sigma_y}\frac{\partial H}{\partial \bar{\varepsilon}^{\mathrm{p}}} + \frac{\partial g}{\partial \tau_{xy}}\frac{\partial H}{\partial \varepsilon'^{\mathrm{p}}}\right). \tag{6}$$

The particular form of A^* is determined using hardening rules and yield function. Various hardening rules come to different plastic modulus [10]. Another important parameter is the plastic flow factor $\mathrm{d}\lambda$. When the material is in an elastic state, $\mathrm{d}\lambda = 0$ and when the material is in an elasto-plastic state, $\mathrm{d}\lambda > 0$. When the material reaches its limit state, $\mathrm{d}\lambda = \infty$ and $\mathrm{d}H = 0$ (i.e. no hardening) and the plastic modulus $A^* = 0$, which implies that the deformation increases infinitely without any increase in stress.

The above constitutive relationships (Eqs. (1)–(6)) can be expressed in the following matrix form:

$$\{\mathrm{d}\boldsymbol{\sigma}\} = ([D]^{\mathrm{e}} - [D]^{\mathrm{p}})\{\mathrm{d}\boldsymbol{\varepsilon}\}, \tag{7}$$

$$[D]^{\mathrm{p}} = \frac{H(l)}{A}[D]^{\mathrm{e}}\left\{\frac{\partial g}{\partial \boldsymbol{\sigma}}\right\}\left\{\frac{\partial f}{\partial \boldsymbol{\sigma}}\right\}^{\mathrm{T}}[D]^{\mathrm{eT}}, \tag{8}$$

$$A = A^* + \left\{\frac{\partial f}{\partial \boldsymbol{\sigma}}\right\}^{\mathrm{T}} [D]^{\mathrm{e}} \left\{\frac{\partial g}{\partial \boldsymbol{\sigma}}\right\}, \tag{9}$$

where $H(l)$ is the Heaviside function, and $l = \left\{\partial g/\partial \boldsymbol{\sigma}\right\}^{\mathrm{T}} \{\mathrm{d}\boldsymbol{\sigma}\}$ and is termed as loading/unloading factor. The criterion for loading/unloading is given as

$$\begin{cases} l > 0,\ \mathrm{d}\lambda > 0, & H(l) = 1 \quad \text{Elasto-plastic deformation,} \\ l \leqslant 0,\ \mathrm{d}\lambda = 0, & H(l) = 0 \quad \text{Elastic or neutral deformation.} \end{cases} \tag{10}$$

For a plane strain problem

$$\{\mathrm{d}\boldsymbol{\sigma}\} = \begin{Bmatrix} \mathrm{d}\sigma_x \\ \mathrm{d}\sigma_y \\ \mathrm{d}\tau_{xy} \end{Bmatrix}, \quad \{\mathrm{d}\boldsymbol{\varepsilon}\} = \begin{Bmatrix} \mathrm{d}\varepsilon_x \\ \mathrm{d}\varepsilon_y \\ \mathrm{d}\gamma_{xy} \end{Bmatrix}, \tag{11}$$

$$[D]^{\mathrm{e}} = \begin{bmatrix} K + \frac{4}{3}G & K - \frac{2}{3}G & 0 \\ K - \frac{2}{3}G & K + \frac{4}{3}G & 0 \\ 0 & 0 & G \end{bmatrix},$$

$$[D]^{\mathrm{p}} = \frac{H(l)}{A} \begin{bmatrix} A_{11} & A_{12} & A_{13} \\ A_{21} & A_{22} & A_{23} \\ A_{31} & A_{32} & A_{33} \end{bmatrix}, \tag{12}$$

where γ_{xy} is the shear strain, ε_x and ε_y are the normal strain along x- and y-directions, respectively, and the A_{ij} terms can be obtained using Eq. (8). If an associated flow rule ($f = g$) is used, A_{ij} is symmetric such that $A_{ij} = A_{ji}$. K and G are the elastic bulk and shear moduli, respectively.

2.2. Consideration of an interface with thickness approaching zero

Fig. 2(a) shows a continuous interface element while Fig. 2(b) shows a discontinuous interface element with thickness b approaching zero and having a distinct jump in both normal and shear displacements at the interface. The limit concept for the deformation, **u**, of a very thin interface element shown in Fig. 2(b) can be expressed mathematically as

$$[[\![\, \mathrm{d}u \,]\!]_J] = [[\![\, \mathrm{d}u_{\mathrm{n}} \,]\!]\ [\![\, \mathrm{d}u_{\mathrm{s}} \,]\!]]^{\mathrm{T}} = \lim_{b\to 0} [b\varepsilon_{\mathrm{n}}\ b\gamma_{\mathrm{sn}}]^{\mathrm{T}}, \tag{13}$$

where $[\![\, \mathrm{d}u_{\mathrm{n}} \,]\!]$ and $[\![\, \mathrm{d}u_{\mathrm{s}} \,]\!]$ denote the increments of normal and shear displacement jumps, respectively. The elastic normal stiffness, K_{n}, and the elastic shear stiffness, K_{s}, are defined as

$$K_{\mathrm{n}} = \frac{\mathrm{d}\sigma_{\mathrm{n}}}{\mathrm{d}[\![\, u_{\mathrm{n}} \,]\!]} = \lim_{b\to 0}\left[\frac{1}{b}\left(K + \frac{4}{3}G\right)\right],$$

$$K_{\mathrm{s}} = \frac{\mathrm{d}\tau_{\mathrm{sn}}}{\mathrm{d}[\![\, u_{\mathrm{s}} \,]\!]} = \lim_{b\to 0}\left[\frac{G}{b}\right], \tag{14}$$

where $\{\mathrm{d}\boldsymbol{\sigma}\} = \{\mathrm{d}\sigma_{\mathrm{n}} \mathrm{d}\tau_{\mathrm{sn}}\}^{\mathrm{T}}$ for an interface, and $\mathrm{d}\sigma_{\mathrm{n}}$ and $\mathrm{d}\tau_{\mathrm{sn}}$ are the normal and shear stress increments, respectively. Following the concept adopted by Desai et al. [7], Eq. (14) should also be applicable to an interface with a finite thickness. Based on the limit concept expressed by Eq. (13), the constitutive equation for an interface with finite thickness can be readily transplanted into that for an interface with thickness b approaching zero. The constitutive law for an interface with b approaching zero is derived as follows:

$$\{\mathrm{d}\boldsymbol{\sigma}\} = ([\bar{D}]^{\mathrm{e}} - [\bar{D}]^{\mathrm{p}})\{[\![\, \mathrm{d}u \,]\!]_J\}, \tag{15}$$

where

$$[\bar{D}]^{\mathrm{e}} = \lim_{b\to 0}\frac{[D]^{\mathrm{e}}}{b} = \begin{bmatrix} K_{\mathrm{n}} & 0 \\ 0 & K_{\mathrm{s}} \end{bmatrix} \quad \text{for plane strain interface,} \tag{16}$$

$$[\bar{D}]^{\mathrm{p}} = \lim_{b\to 0}\frac{[D]^{\mathrm{p}}}{b} = \frac{1}{\bar{A}}[\bar{D}]^{\mathrm{e}} \left\{\frac{\partial g}{\partial \boldsymbol{\sigma}}\right\} \left\{\frac{\partial f}{\partial \boldsymbol{\sigma}}\right\}^{\mathrm{T}} [\bar{D}]^{\mathrm{eT}}, \tag{17}$$

$$\bar{A} = \lim_{b\to 0}\frac{A}{b} = \bar{A}^* + \left\{\frac{\partial f}{\partial \boldsymbol{\sigma}}\right\}^{T} [\bar{D}]^{\mathrm{e}} \left\{\frac{\partial g}{\partial \boldsymbol{\sigma}}\right\},$$

$$\bar{A}^* = \lim_{b\to 0}\frac{A^*}{b} = (-)\frac{\partial f}{\partial H}\left(\frac{\partial g}{\partial \sigma_{\mathrm{n}}}\frac{\partial H}{\partial [\![\, u_{\mathrm{n}} \,]\!]} + \frac{\partial g}{\partial \tau_{\mathrm{sn}}}\frac{\partial H}{\partial [\![\, u_{\mathrm{s}} \,]\!]}\right). \tag{18}$$

A particular form of yield function is proposed and associated flow rule is applied.

$$f = \frac{(\sigma_n - \gamma H)^2}{C} + \frac{\tau_{\mathrm{sn}}^2}{B\alpha^2(\theta)} - H^2 = 0 \quad (f = g). \tag{19}$$

A hardening rule is assumed to be of the following form which is obtained through the normalized plastic work (refer to Section 3.2 for further details):

$$H = H(h) = H(m_1 + m_2[\![\, u_{\mathrm{n}} \,]\!] + m_3[\![\, u_{\mathrm{s}} \,]\!]\alpha(\theta)), \tag{20}$$

$$h = m_1 + m_2[\![\, u_{\mathrm{n}} \,]\!] + m_3[\![\, u_{\mathrm{s}} \,]\!]\alpha(\theta), \tag{21}$$

where $B, C, \gamma, m_1, m_2, m_3$ are model parameters, $\alpha(\theta)$ is a shape function denoting the effect of shear direction, θ is the shear direction angle and h is the equivalent relative displacement representing the combined effect of both shear and normal displacements. The model parameters and shape function will be further elaborated in Section 3. The general stress–displacement relation for an interface can then be derived as follows:

$$\begin{Bmatrix} \Delta\sigma_{\mathrm{n}} \\ \Delta\tau_{\mathrm{sn}} \end{Bmatrix} = [D]_{\mathrm{ep}} \begin{Bmatrix} [\![\, \Delta u_{\mathrm{n}} \,]\!] \\ [\![\, \Delta u_{\mathrm{s}} \,]\!] \end{Bmatrix}, \tag{22}$$

$$[D]_{\mathrm{ep}} = \begin{bmatrix} K_{\mathrm{n}} - \frac{H(l)}{\bar{A}}\frac{4}{C^2}K_{\mathrm{n}}^2(\sigma_{\mathrm{n}} - \gamma H)^2 & -\frac{H(l)}{\bar{A}}\frac{4K_{\mathrm{s}}K_{\mathrm{n}}}{BC}(\sigma_{\mathrm{n}} - \gamma H)\frac{\tau_{\mathrm{sn}}}{\alpha(\theta)} \\ -\frac{H(l)}{\bar{A}}\frac{4K_{\mathrm{s}}K_{\mathrm{n}}}{BC}(\sigma_{\mathrm{n}} - \gamma H)\frac{\tau_{\mathrm{sn}}}{\alpha(\theta)} & K_{\mathrm{s}} - \frac{H(l)}{\bar{A}}\frac{4K_{\mathrm{s}}^2}{B^2}\frac{\tau_{\mathrm{sn}}^2}{\alpha^2(\theta)} \end{bmatrix}, \tag{23}$$

$$\bar{A} = \frac{4}{C^2}(\sigma_{\mathrm{n}} - \gamma H)^2 K_{\mathrm{n}} + \frac{4}{B^2}K_{\mathrm{s}}\frac{\tau_{\mathrm{sn}}^2}{\alpha^2(\theta)} + \bar{A}^*, \tag{24}$$

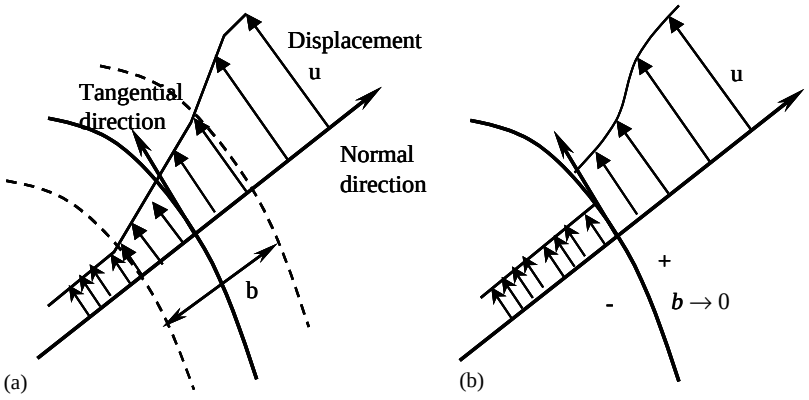

Fig. 2. (a,b) Limit concept from continuity to discontinuity.

$$\bar{A}^* = \frac{4}{C}[\gamma\sigma_n + (C-\gamma^2)H]\left[m_2\frac{\sigma_n-\gamma H}{C} + m_3\frac{\tau_{sn}}{B\alpha(\theta)}\right]\frac{dH}{dh}. \tag{25}$$

The failure criterion $\bar{A}^* = 0$ implies that

$$\frac{\tau_{sn}}{\sigma_n\alpha(\theta)} = M \rightarrow \text{Mohr}-\text{Coulomb Law}, \tag{26}$$

where M is a constant determined by model parameters. Eq. (26) indicates that the characteristics of an interface is frictional in nature and generally follows the Mohr–Coulomb law during shearing. The loading/unloading factor in this case can be expressed as

$$l = \frac{2}{C}(\sigma_n - \gamma H)\,d\sigma_n + \frac{2}{B}\frac{\tau_{sn}}{\alpha^2(\theta)}\,d\tau_{sn}. \tag{27}$$

Two special cases, constant normal stress ($\sigma_n =$ Constant) and constant normal displacement ($[\![u_n]\!] =$ Constant), will be examined here as existing experimental data [1,4,8,11] on joint testing under such conditions are available to verify the above constitutive model. For simplification, shear anisotropy is not considered for the two cases. That is $\alpha(\theta) \equiv 1$. An assumption is also made for the motion of yield function, that is $\gamma \equiv 1$.

2.3. Constant normal force

At this state, the normal stress increment $\Delta\sigma_n$ is zero. The increment of shear stress $\Delta\tau_{sn}$ is derived from Eq. (22) as follows:

$$\Delta\tau_{sn} = \left\{K_s - H(l)\frac{4K_s^2\tau_{sn}^2}{\bar{A}B}\left[\frac{1}{B} + \frac{4K_n(\sigma_n-H)^2}{C^2\left(\frac{4}{B}K_s\tau_{sn}^2 + B\bar{A}^*\right)}\right]\right\}[\![\Delta u_s]\!]. \tag{28}$$

The dilatancy of an interface is represented by the relationship between normal and shear displacements and can be represented by

$$[\![\Delta u_n]\!] = \begin{cases} \dfrac{4K_s(\sigma_n - H)\tau_{sn}}{C\left(\frac{4K_s}{B}\tau_{sn}^2 + B\bar{A}^*\right)}[\![\Delta u_s]\!] & \text{upon elasto-plastic loading,} \\ 0 & \text{other cases.} \end{cases} \tag{29}$$

2.4. Constant normal displacement

The normal deformation of an interface is sometimes constrained by the surrounding rock mass. This constraint can be expressed as

$$[\![\Delta u_n]\!] = 0. \tag{30}$$

At this state, the normal and shear stress responses are

$$\Delta\sigma_n = -H(l)\frac{4K_sK_n}{\bar{A}BC}(\sigma_n - H)\tau_{sn}[\![\Delta u_s]\!], \tag{31}$$

$$\Delta\tau_{sn} = \left\{K_s - H(l)\frac{4}{\bar{A}}\frac{K_s^2}{B^2}\tau_{sn}^2\right\}[\![\Delta u_s]\!]. \tag{32}$$

The stress ratio, $\Delta\sigma_n/\Delta\tau_{sn}$, can then be derived from the above two equations

$$\frac{\Delta\sigma_n}{\Delta\tau_{sn}} = -\frac{4H(l)K_n(\sigma_n - H)\tau_{sn}}{BC\left\{\bar{A} - H(l)\frac{4}{B^2}K_s\tau_{sn}^2\right\}}. \tag{33}$$

3. Model parameters

The parameters required for the present model include those concerning normal and shear displacement and anisotropy. These parameters are listed in Table 1 and their definitions and derivations are described in this section. Illustrations on the determination of these parameters from experimental data will be presented in Section 4.

3.1. Shear and normal stiffness parameters

Bandis et al. [1] performed tests on limestone and dolerite joints with no shear anisotropy. Fig. 3 shows that a linear relationship exists between the normal stress and elastic shear stiffness (=force/displacement) for all test cases. Similar observations were also made by other researchers [4, 8]. Thus the elastic shear stiffness K_s is a function of normal stress at the interface and can be expressed in terms of

$$\frac{K_s}{\alpha(\theta)} = \begin{cases} K_{s0} + a_1\sigma_n, & \sigma_n \geqslant 0, \\ 0, & \sigma_n < 0. \end{cases} \tag{34}$$

When the joint interface is open ($[\![u_n]\!] < 0$ or $\sigma_n < 0$), the elastic shear stiffness should be zero. The shape function $\alpha(\theta)$ is introduced to the elastic shear stiffness to consider the effect of shear anisotropy in elastic deformation. As Bandis et al.'s tests did not involve any shear anisotropy, the magnitude of the shape function is unity. The shear elasticity parameters K_{s0} and a_1 can be directly determined from the y-intercept and the gradient of the best straight line for the elastic shear stiffness – normal stress responses for a particular rock joint interface, respectively, see Fig. 3.

Table 1
Constitutive model parameters

Shear elasticity	K_{s0}, a_1
Normal elasticity	K_{n0}, V_{sm}
Normal compression	a, b
Equivalent	$m_2, m_{30}, m_{31}, m_{32}$
Shape	B, C, γ
Anisotropy	A_1, A_2, σ_c, ϕ

For the normal stress/displacement response, it is found that approximately linear relationships exist where the normal displacement is plotted against normal displacement/normal stress for both loading and unloading stages, as shown in Fig. 4. Thus the normal stress/displacement response is non-linear. The following relationship is proposed to determine the elastic normal stiffness K_n from the unloading stage of the normal stress/displacement response:

$$K_n = \begin{cases} \dfrac{K_{n0}}{\left(1 - [\![u_n]\!]/V_{sm}\right)^2}, & 0 < [\![u_n]\!] \leqslant V_{sm}, \\ 0, & [\![u_n]\!] \leqslant 0, \end{cases} \tag{35}$$

where K_{n0} is the initial normal stiffness when normal stress is zero and V_{sm} is the maximum normal displacement measured from zero normal stress state. The two parameters can be obtained from the unloading line shown in Fig. 4.

The loading stage of the normal stress/displacement responses can be represented by a hyperbolic relationship given as

$$\sigma_n = P_a \frac{h_*}{a - bh_*} \tag{36}$$

where h_* is the normal displacement under normal stress only. The normal compression parameters a and b can be obtained from the loading line shown in Fig. 4.

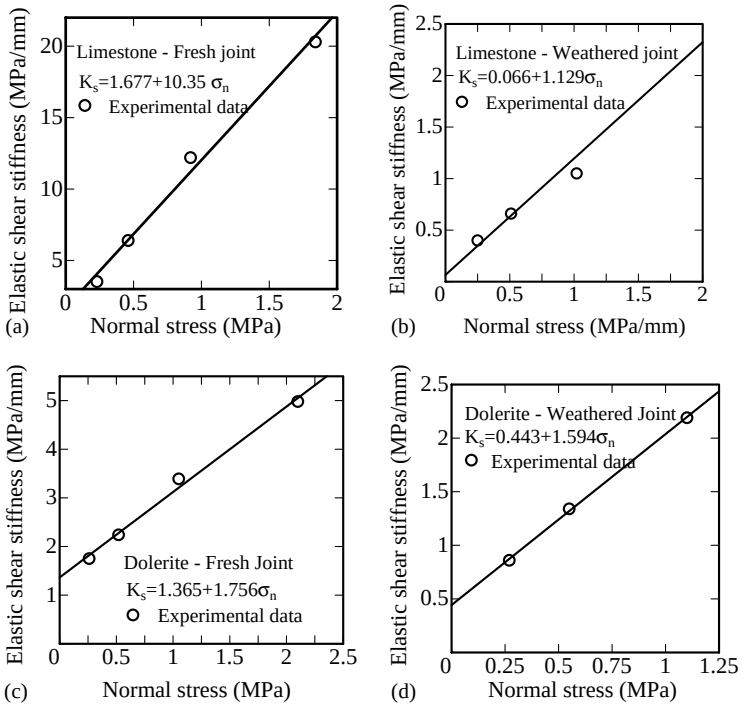

Fig. 3. (a–d) Variation of elastic shear stiffness with normal stress (solid line represents the best straight-line fit, experimental data from [1]).

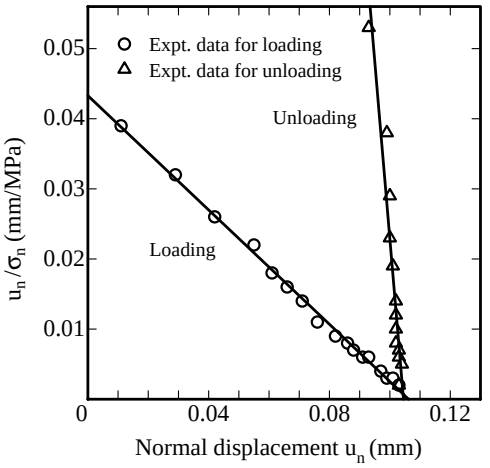

Fig. 4. Variation of normal displacement/normal stress versus normal displacement for fresh limestone joint [1].

3.2. Hardening rule

In this section, the following notations are introduced. The mean stress $\bar{\sigma} = (1/3)\sigma_{ii}$; the derivatoric stress $\sigma'_{ij} = \sigma_{ij} - \bar{\sigma}\delta_{ij}$; the mean strain $\bar{\varepsilon} = (1/3)\varepsilon_{ii}$; the volumetric strain is $3\bar{\varepsilon}$; and the derivatoric strain, $\varepsilon'_{ij} = \varepsilon_{ij} - \bar{\varepsilon}\delta_{ij}$. In addition, ε^{p}_{vd} and ε^{p}_{vc} are plastic volumetric strains induced by shear stress and mean stress, respectively.

Moroto [12] established the following relation for normalized plastic work on sand

$$\bar{\sigma}\,\mathrm{d}\varepsilon^{p}_{vd} + \sigma'_{ij}\,\mathrm{d}\varepsilon'^{p}_{ij} = \bar{\sigma}\alpha(\theta)\omega(\xi)\,\mathrm{d}\xi \quad \text{where } \mathrm{d}\xi = \|\mathrm{d}\varepsilon'^{p}_{ij}\|, \tag{37}$$

where $\omega(\xi)$ is a parameter independent of relative density, mean stress, stress path, over-consolidation ratio and inherent anisotropy [13]. In the present study, σ'_{ij} and $\mathrm{d}\varepsilon'^{p}_{ij}$ are assumed to be co-axial:

$$\sigma'_{ij}\,\mathrm{d}\varepsilon'^{p}_{ij} = \|\sigma'_{ij}\|\,\|\mathrm{d}\varepsilon'^{p}_{ij}\|. \tag{38}$$

Then

$$\mathrm{d}\varepsilon^{p}_{vd} = \left[\alpha(\theta)\omega(\xi) - \frac{\|\sigma'_{ij}\|}{\bar{\sigma}}\right]\mathrm{d}\xi. \tag{39}$$

The asperity angle, α_i, is defined as

$$\tan(\alpha_i) = \frac{\mathrm{d}\varepsilon^{p}_{vd}}{\mathrm{d}\xi}. \tag{40}$$

Thus α_i approaches zero when shear deformation increases. In fact, Eq. (39) is the equation representing dilatancy of the interface. The plastic volumetric strain increment $\mathrm{d}\varepsilon^{p}_{vc}$ consists of two parts: one ($3\mathrm{d}\bar{\varepsilon}^{p}$) for compression and the other for dilatancy:

$$\mathrm{d}\varepsilon^{p}_{vc} = 3\,\mathrm{d}\bar{\varepsilon}^{p} + \left[\frac{\|\sigma'_{ij}\|}{\bar{\sigma}} - \alpha(\theta)\omega(\xi)\right]\mathrm{d}\xi. \tag{41}$$

To transplant Eq. (41) that is appropriate for sand to a case that is appropriate for an interface with thickness approaching zero, the following replacement of parameters is made:

$$\begin{aligned} &3\mathrm{d}\bar{\varepsilon}^{p} \to \mathrm{d}[\![\,u_n\,]\!],\\ &\mathrm{d}\xi \to \mathrm{d}[\![\,u_s\,]\!],\\ &\mathrm{d}\varepsilon^{p}_{vc} \to \mathrm{d}h. \end{aligned} \tag{42}$$

The equivalent relative displacement, h, is employed to express the combined effect of shear and normal displacements of an interface and represented by Eq. (21). With the replacement of parameters indicated by Eq. (42), the equivalent relative displacement increment, $\mathrm{d}h$, can be obtained as

$$\mathrm{d}h = \mathrm{d}[\![\,u_n\,]\!] + \left[\frac{\|\sigma'_{ij}\|}{\bar{\sigma}} - \alpha(\theta)\omega(\xi)\right]\mathrm{d}[\![\,u_s\,]\!]. \tag{43}$$

The equivalent relative displacement, h, can be derived by integrating Eq. (43):

$$h = [\![\,u_n\,]\!] + \left[\frac{\|\sigma'_{ij}\|}{\bar{\sigma}} - \alpha(\theta)\omega(\xi)\right]_{\mathrm{mean}}[\![\,u_s\,]\!]. \tag{44}$$

The equivalent relative displacement is obtained from the normalized plastic work, which describes a direction-dependent hardening rule using shape function $\alpha(\theta)$. In this respect, parameter m_1 expresses the hardening parameter before initial stress while m_2 is the amplified coefficient for normal displacement. The parameter m_3, which represents the dilatancy state that approaches to zero at the limit state [14], is expressed in terms of normal stress and displacement as follow:

$$m_3 = (m_{30} + m_{31}\sigma_n)\,\mathrm{e}^{-m_{32}[\![\,u_s\,]\!]}, \tag{45}$$

where m_{30}, m_{31}, m_{32} are terms as equivalent parameters. The parameter m_{32} is introduced to describe the non-linearity of asperity under shear deformation. When the shear deformation is sufficiently large, asperity m_3 should be zero.

3.3. Anisotropy parameter $\alpha(\theta)$

Anisotropy refers to the property changes of an interface along different shear loading directions. Referring to Eq. (26), the anisotropy parameter $\alpha(\theta)$ is directly associated with the anisotropy of shear strength (i.e. friction angle) of the interface. The friction angle of an interface has the following characteristics [4,11]. Firstly, the magnitude of friction angle depends on both shear direction and normal stress. The shear direction-dependency decreases with an increase of normal stress. Under high normal stress, shear anisotropy is relatively insignificant, as illustrated in Fig. 5. Secondly, the directional distribution of friction angle under a constant normal stress is symmetrical along certain shear direction. The symmetry axis may rotate gradually with an increase of normal stress, and the extent of anisotropy becomes weaker and weaker. The shear anisotropy can be described by the following ellipse

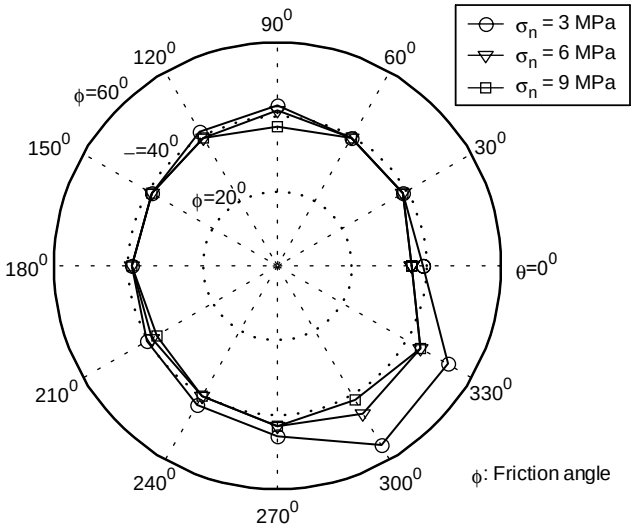

Fig. 5. Polar plot of friction angle of interface versus shear direction angle θ (from Ref. [4]).

function:

$$\alpha_t(\theta) = \cos(\theta - \Psi),$$
$$\alpha_s(\theta) = (1 + A_0)\sin(\theta - \Psi), \tag{46}$$

$$A_0 = A_1\left(1 - \frac{\sigma_n}{\sigma_c}\right)^{A_2}, \tag{47}$$

where σ_c is the uniaxial compressive strength of intact rock. The joint is completely closed when $\sigma_n = \sigma_c$. In addition, $A_0 = 0$ ($A_1 \equiv 0$) implies no shear anisotropy. Ψ is an inclination angle of anisotropy with respect to the local co-ordinates of shear plane.

3.4. Shape parameters

The kinetic parameter, γ, is introduced to describe the transition zone between the initial and the final limit state:

$$\gamma = 1 + \sqrt{\frac{[\![u_s]\!]}{[\![u_c]\!]}}\left(\frac{\sigma_n}{H} - 1\right). \tag{48}$$

Thus $\gamma = 1$ at the initial state and zero at the limit state.

Shape parameters B and C are introduced to describe the flow direction, χ, of yield function as follows:

$$\chi = -\frac{d[\![u_n]\!]}{d[\![u_s]\!]} = \frac{B}{C}\eta + \frac{B}{C(C-1)} \times \left[-\eta + \sqrt{\eta^2 C + \frac{C(C-1)}{B}}\right], \quad \eta = \frac{\sigma_n}{\tau_{sn}}. \tag{49}$$

Thus χ is a function of η but is independent of hardening function H. The parameters B and C can be obtained by curve fitting on the plot of χ versus η.

4. Verification of model

In this section, the validity of the model is evaluated using existing experimental data on joints by Bandis et al. [1], Desai and Fisherman [2] and Jing [4]. The first two involved tests on joints with no shear anisotropy while the last one involved testing of concrete replica of natural granite joints with shear anisotropy.

4.1. Comparison with data of Bandis et al

One of the tests performed by Bandis et al. [1] was a fresh limestone joint with joint compressive strength $JCS = 154$ MPa and joint roughness coefficient $JRC = 11.8$. The shear elasticity parameters K_{s0} and a_1 can be obtained from Fig. 3(a) while the normal elasticity parameters K_{s0} and V_{sm} and the normal compression parameters a and b can be obtained from the unloading and loading stages of the test data shown in Fig. 4, respectively. From the equivalent hardening rule, the parameters m_2 and m_3 can be determined. The equivalent parameters, m_{30} and m_{31}, can be obtained using Eq. (45) based on the m_3 versus σ_n plot shown in Fig. 6. The best fitting method is used to determine the shape parameters B and C on the flow direction of deformation using Eq. (49). The kinematic parameter γ is taken as 1 for simplification. As there was no shear anisotropy in the joint tests, $A_1 = 0$ and the anisotropy parameters are not required. The magnitudes of all the model parameters are listed in Table 2.

The parameters are used as input in the present model to simulate the normal and shear responses of the joint rocks as shown in Figs. 7 and 8. In general, the predicted and observed responses are in reasonably good agreement. It is noted that the shear responses are non-linear and the ultimate shear strength increases with normal stress. Therefore, the nonlinearity of an interface can be

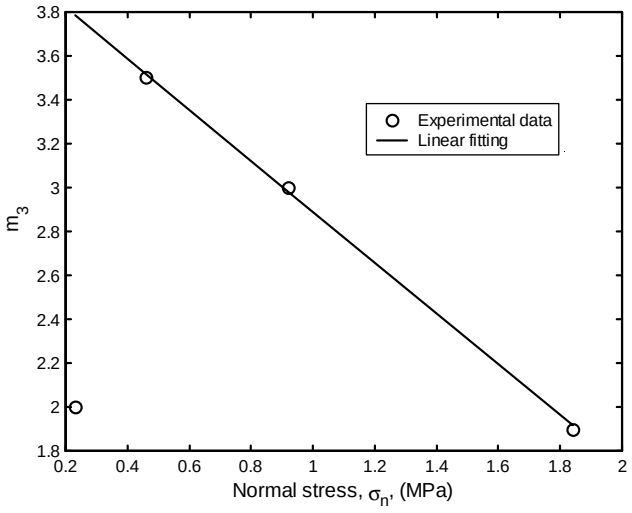

Fig. 6. Variation of m_3 with normal stress.

Table 2
Constitutive model parameters for Bandis et al.'s experimental data

K_{s0} (MPa)	a_1	K_{n0} (MPa)	V_{sm} (mm)	a (mm)	b	m_2	m_{30}	m_{31} (MPa^{-1})
1.677	10.35	18.9	0.105	0.0433	0.408	2.05	4.05	−1.16
m_{32}	B	C	γ	A_1	A_2	σ_c (MPa)	Ψ (deg)	
0.5	1.69	1.40	1	0.0	—	—	—	

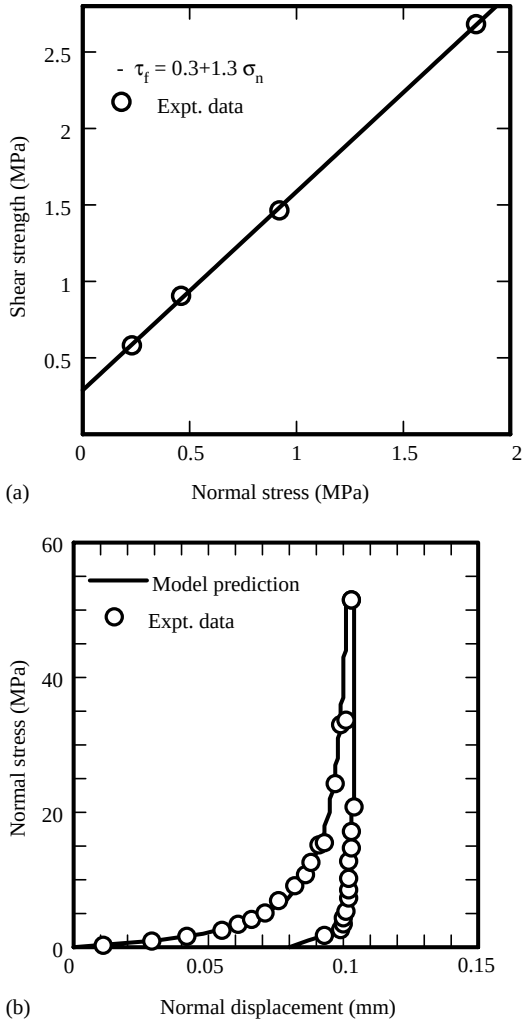

Fig. 7. (a,b) Prediction for shear strength and normal stress/displacement response (for Bandis et al.'s experimental data [1]).

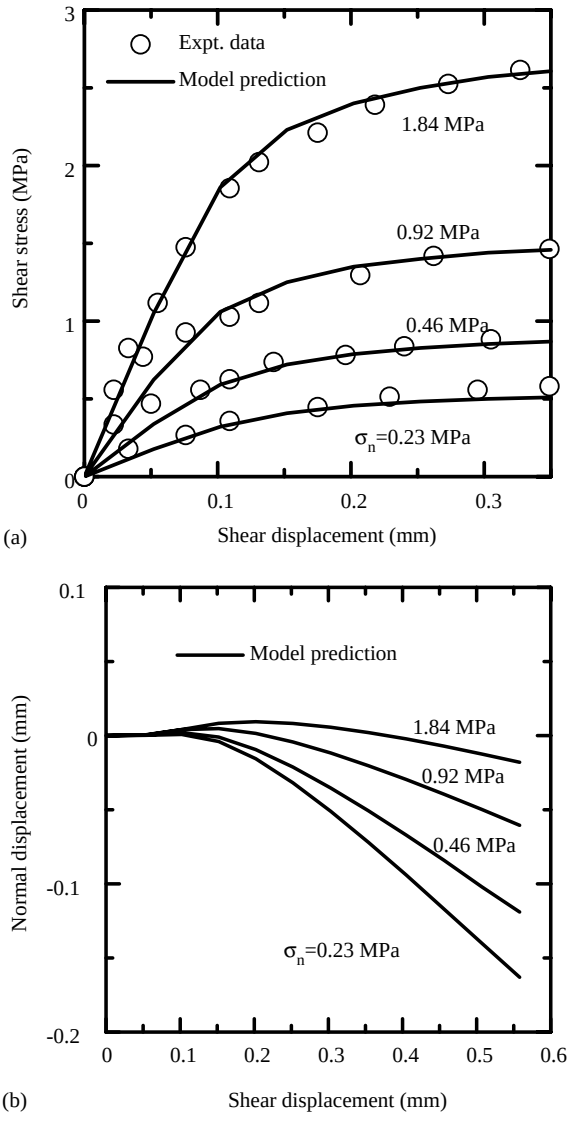

Fig. 8. (a,b) Prediction for shear stress/displacement and normal/shear displacement responses (for Bandis et al.'s experimental data [1]).

established as normal stress-dependent, which is typical for a frictional material. The dilatancy is restrained by the increase of normal stress as shown in Fig. 8(b). The bigger the normal stress, the smaller is the normal displacement. Fig. 8(b) illustrates the output of Eq. (29) when γ is taken as 1. It is evident that the model overestimates the dilatancy especially under small normal stress. In addition, the normal displacement should approach to the same asymptotic value when the shear deformation is sufficiently large. This is because the asperity of joints is completely damaged

($[\![\Delta u_n]\!] = 0$) upon reaching the limit state. Thus in the present constitutive model, two constants, γ and m_3, are sensitive to the dilatancy. The present computation shows that the smaller the m_3, the higher is the joint strength and less dilatancy.

Associated flow rule is used in the present constitutive model and thus the stiffness matrix of the interface is symmetric. As associated flow rule usually predicts higher dilatancy than non-associated flow rule, the present model introduces non-homogeneous motion of center and hardening rule. These two parameters help to improve the accuracy of the prediction capability of the present model even when associated flow rule is used, as illustrated in the above example. As the present model treats the friction process (sliding) as a plastic deformation, it has the same capability as the non-associated flow rule to predict the irreversibility of the friction process.

4.2. Comparison with data of Desai and Fishman

Desai and Fishman [2] evaluated the behavior of joints using concrete samples with no shear anisotropy. Here only the experimental data with asperity angle $\alpha = 7^\circ$ is used to validate the present model. The model parameters are determined using the same approach described in Section 4.1. As illustrative examples, the elastic shear stiffness parameters K_{s0} and a_1 can be determined from Fig. 9(a) while the equivalent parameters m_{30} and m_{31} can be determined from Fig. 9(b). m_{32} is assumed in this computation. The magnitudes of all the model parameters are given in Table 3.

Using the model parameters as input in the present model, simulations are carried out to predict the shear and normal responses of the joint under constant normal stress, as shown in Figs. 10(a) and (b). For most cases, the predicted shear stress is marginally lower than the experimental data at the same shear displacement. For all cases, the shear stress/displacement responses exhibit two distinct zones. The first is the relatively short elastic zone when the shear displacement is less than 0.5 mm. Thereafter, a fairly abrupt change to the relatively long plastic zone is noted where there is a large increase in shear displacement without any significant increase in shear stress. It is worthy to note that the shear stress/displacement response of the interface for both the elastic and plastic zones can be predicted reasonably well using the present model. On the other hand, the normal/shear displacement responses exhibit a gradual transition from the elastic to plastic zones. The predicted responses agree reasonably well with the measured responses for the test with $\sigma_n = 138$ kPa, as shown in Fig. 10(b). However, the comparison between the predicted and measured responses for the test with $\sigma_n = 69$ kPa is not as promising. This is probably attributed to the less reliable

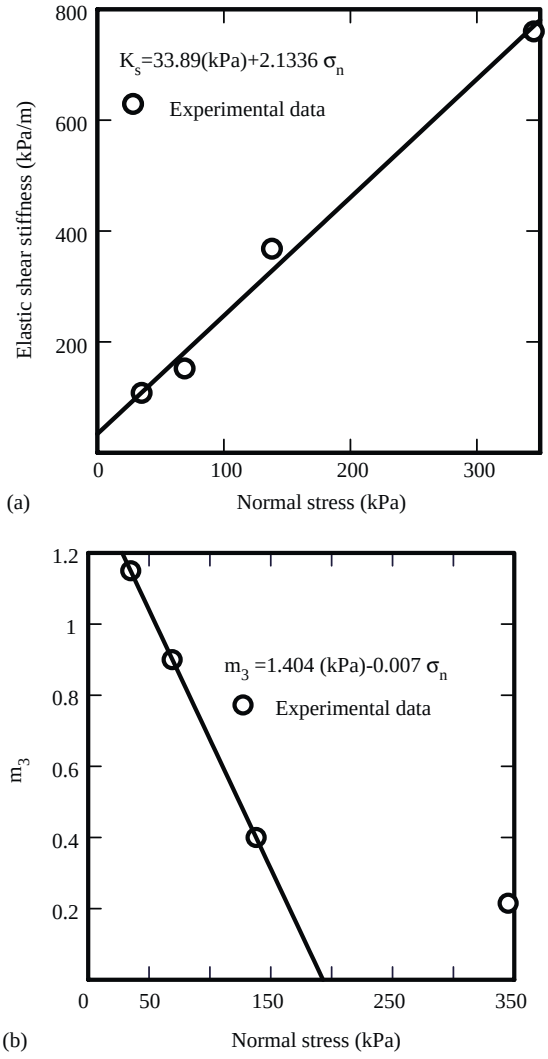

Fig. 9. (a,b) Determination of selected model parameters (Desai and Fishman's experimental data [2]).

measured data in the early stage of the test. The last few measured data points for both tests shown in Fig. 10(b) reveal that the normal displacement has not reached an asymptotic value while the present model predicts an asymptotic value when the shear deformation is large. This illustrates that dilatancy of an interface is a difficult process to model accurately.

4.3. Comparison with data of Jing

Jing [4] tested concrete replicas of natural granite joints in a servo-controlled direct shear box. The test data are chosen as the tests involved joints with shear anisotropy. The concrete material has following composition by weight (%): Portland cement, 31.2; microsilica 4.7; water 7.0; super-plastizer 0.4; fine sand (mean grain size = 0.15 mm) 4.7; and coarse sand (mean grain size = 0.30 mm) 52.0. The concrete samples have a mean Young's modulus of 24.4 GPa, Poisson's ratio of 0.26,

Table 3
Constitutive model parameters for Desai and Fishman's experimental data

K_{s0} (MPa)	a_1	K_{n0} (MPa)	V_{sm} (mm)	a (mm)	b	m_2	m_{30}	m_{31} (MPa^{-1})
33.89	2.134	18.9	0.105	0.0433	0.408	2.05	1.404	−0.007
m_{32}	B	C	γ	A_1	A_2	σ_c (MPa)	Ψ (deg)	
0.25	1.69	2.40	1	0.0	—	—	—	

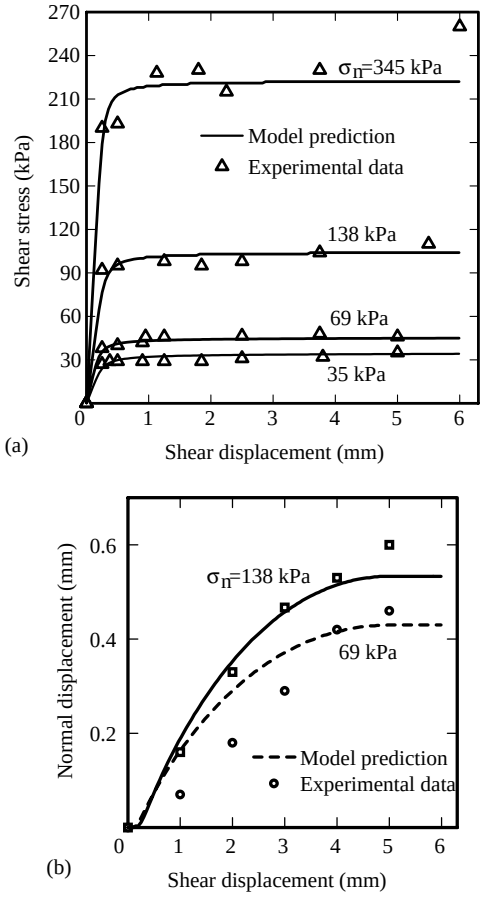

Fig. 10. (a,b) Prediction of shear stress/displacement and normal/shear displacement responses for Desai and Fishman's experimental data [2].

and a uniaxial compressive strength of 52 MPa after 28 days of curing in water. Each sample consists of two blocks with circular cross sections. The lower block is larger than the upper so that it maintains a constant nominal contact area during shear tests. A total of 12 groups of samples were tested under constant normal stress of 1, 3, 6, 9 or 12 MPa to study the behavior of joints subjected to shear anisotropic loading.

The experimental results shown in Fig. 11(a) confirmed that the elastic stiffness is anisotropic as its magnitude changes considerably with shear direction angle. By back analyzing the experimental data, a plot of A_0 versus $(1-\sigma_n/\sigma_c)$ can be obtained and the plot is shown in Fig. 11(b) from which the anisotropic parameters A_1 and A_2 can be obtained. Other model parameters are determined from the experimental data with $\theta = 30^\circ$. The magnitudes of all the model parameters are given in Table 4.

Using the model parameters as input, the predicted shear stress/displacement responses for $\theta = 30^\circ$, 60°, 90°, 120° and 150° are shown in Figs. 12(a)–(e), respectively. It is evident that the predicted responses agree fairly well with the measured values for most cases. The reasonably good agreement verifies that the present model can predict the behavior of joints subjected to shear anisotropic loadings.

5. Conclusion

In this paper, a constitutive model based on the limit concept is developed for rock interfaces and joints. A particular elasto-plastic model is proposed for the interface using a non-proportional ellipse yield function that is different from the conventional yield functions adopted in soil mechanics [15]. The motion of yield function in stress space is governed by its center position and hardening rule. The interface model generally follows the Mohr–Coulomb law at its limit state. Associated flow rule is adopted in the model and a shape function is introduced to incorporate shear anisotropy. Derivations of the constitutive model have been given in detail in this paper.

The present constitutive model essentially employs a number of model parameters in terms of normal and shear stresses and displacements, and shape function. The results of three experimental studies on natural and artificial rock joints are employed to evaluate the validity of the present model. The first two cases involved rock joints with no shear anisotropy while the last case involved rock joints subject to shear anisotropy. The method of determination of standard model parameters based on basic experimental data such as the elastic shear stiffness versus normal stress

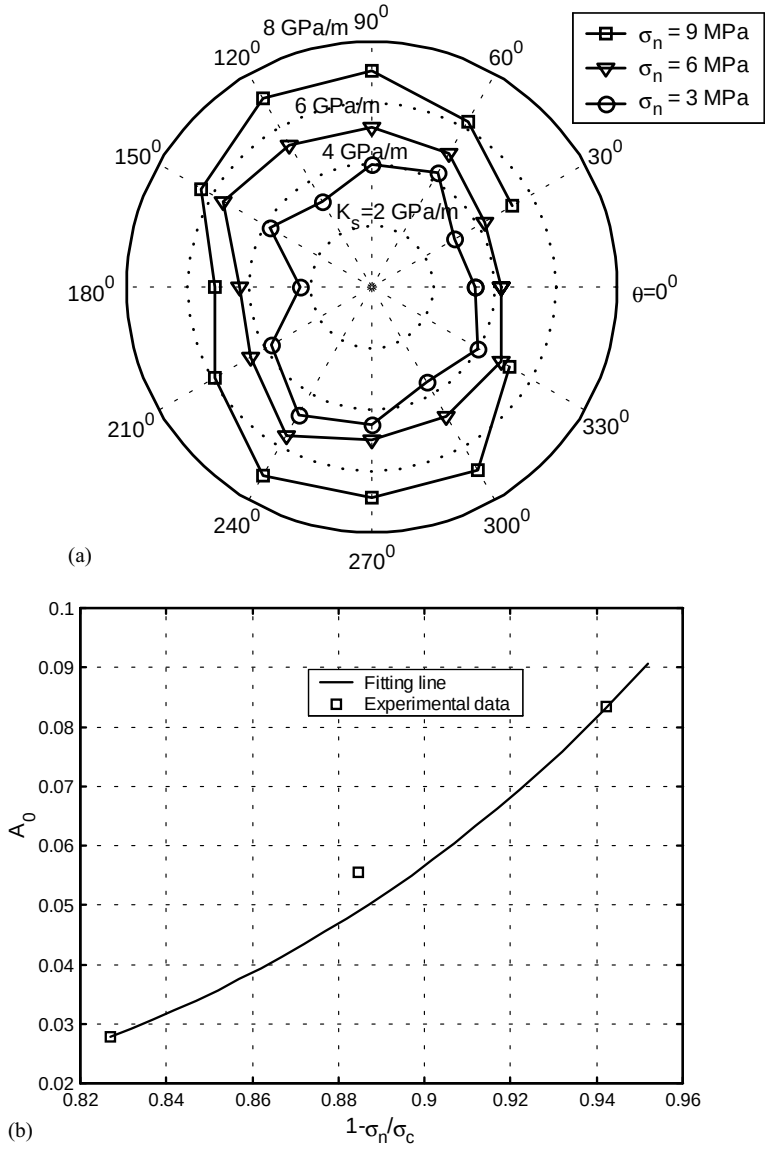

Fig. 11. Determination of parameters for anisotropy (Jing's experimental data [4]). (a) Polar plot of elastic shear stiffness versus shear direction angle θ and (b) Anisotropy parameters.

Table 4
Constitutive model parameters for Jing's experimental data

K_{s0} (MPa)	a_1	K_{n0} (MPa)	V_{sm} (mm)	a (mm)	b	m_2	m_{30}	m_{31} (MPa^{-1})
2.053	0.36	18.9	0.105	0.0433	0.408	3.05	7.76	−0.77
m_{32}	B	C	γ	A_1	A_2	σ_c (MPa)	Ψ (deg)	
0.25	1.8	1.20	1	0.1373	8.41	52	90	

responses is illustrated using the first case while the determination of model parameters involving shear anisotropy is demonstrated using the last case. Using the model parameters as input in the present model, it is established that the predicted shear and normal responses of rock interfaces generally agree reasonably well with the measured data with the exception of shear softening. Although strictly speaking non-associated flow rule should be used in the analysis, the use of such flow rule can run into numerical difficulties at times. In

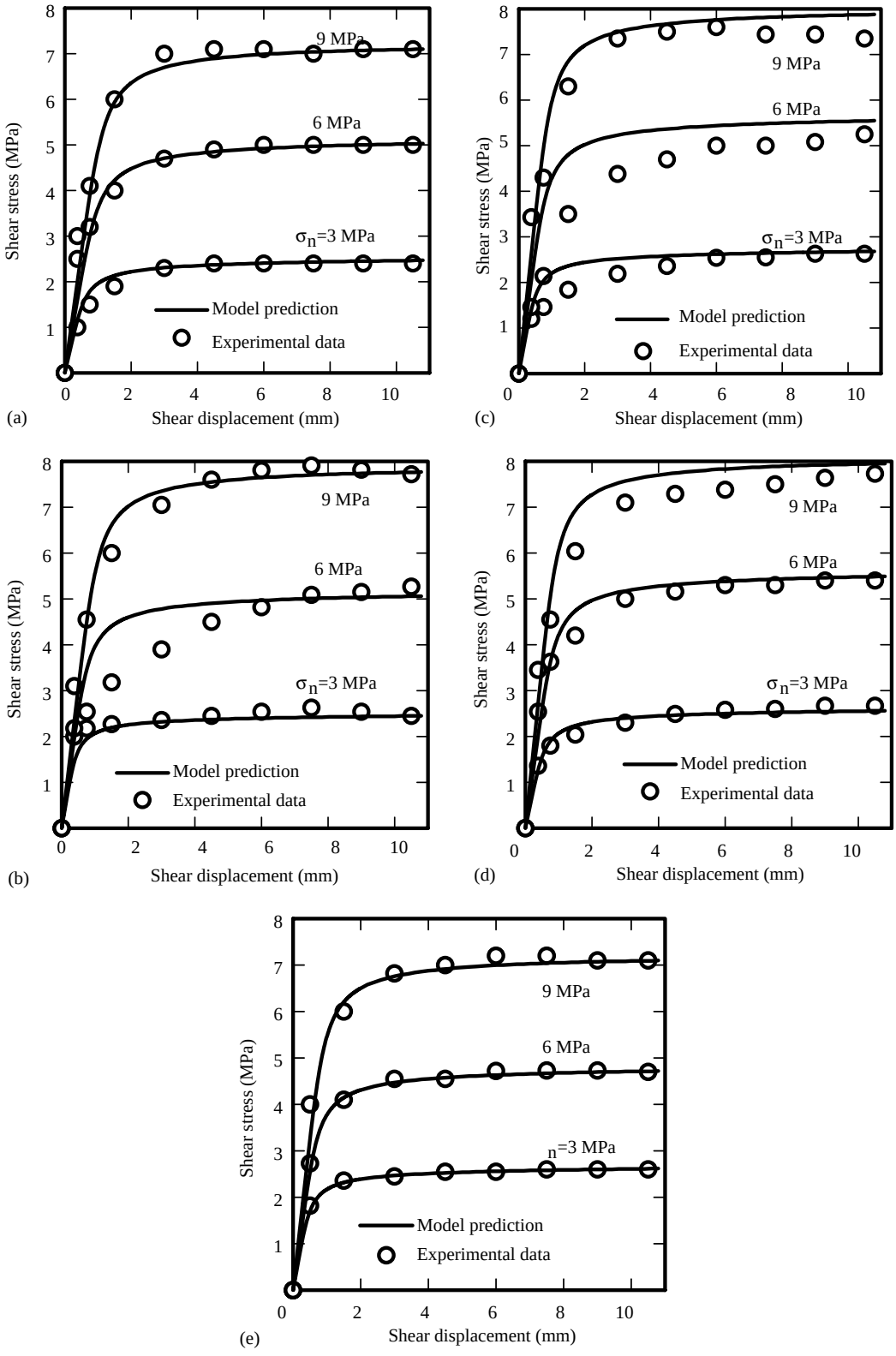

Fig. 12. Response prediction along different shear direction angles (a) $\theta = 30^\circ$, (b) $\theta = 60^\circ$, (c) $\theta = 90^\circ$, (d) $\theta = 120^\circ$ and (e) $\theta = 150^\circ$.

the present study, the adoption of associated flow rule incorporating non-homogeneous motion of center and hardening rule is reasonable judging from the reasonably good agreement between the measured and predicted responses of the rock interface for all the three cases.

References

[1] Bandis SC, Barton NR, Lumsden AC. Fundamentals of rock joint deformation. Int J Rock Mech Min Sci Geomech Abstr 1983;20:249–68.

[2] Desai CS, Fishman KL. Plasticity-based constitutive model with associated testing for joints. Int J Rock Mech Min Sci Geomech Abstr 1991;28(1):15–26.

[3] Uesugi M, Kishida H, Tsubakihara Y. Behavior of sand particles in sand-steel friction. Soils Found 1988;28(1):107–18.

[4] Jing L. Numerical modelling of jointed rock masses by distinct element method for two, and three-dimensional problems. PhD thesis, Lulea University of Technology, 1990.

[5] Clough GW, Duncan JM. Finite element analysis of retaining wall behaviour. J Soil Mech Found Eng 1971; 97(SM12):1657–74, ASCE.

[6] Desai CS, Ma Y. Modeling of joints and interfaces using the disturbed-state concept. Int J Numer Anal Meth Geomech 1992;16:623–53.

[7] Desai CS, Zaman MM, Lightner JG, Siriwardane HJ. Thin-layer element for interfaces and joints. Int J Numer Anal Meth Geomech 1984;8(1):19–43.

[8] Goodman RE. Methods of geological engineering in discontinuous rocks. San Francisco: West Publishing Company, 1976.

[9] Sharma KG, Desai CS. Analysis and implementation of thin-layer element for interfaces and joints. J Eng Mech 1992;118(12): 2442–62.

[10] Huang WX, Pu JL, Chen YJ. Hardening rule and yielding function for soils. Proceedings of the Xth International Conference on Soil Mechanics and Foundation Engineering, Stockholm, 1981.

[11] Arora VK. Strength and deformational behaviour of jointed rocks. PhD thesis, Indian Institute of Technology, India, 1987.

[12] Moroto N. A new parameter to measure degree of shear deformation of granular material in triaxial compression tests. Soils Found 1976;16(4):1–9.

[13] Momen H, Ghaboussi J. Stress dilatancy and normalized work in sands. Proceedings of the IUTAM Symposium on Deformation and Failure of Granular Materials, Delft, The Netherlands, 1982.

[14] Plesha ME. Constitutive models for rock discontinuities with dilatancy and surface degradation. Int J Numer Anal Meth Geomech 1987;11:345–62.

[15] Li G. A study of three-dimensional constitutive relationship of soils and an examination of various models. PhD thesis, Tsinghua University, 1985.

[16] Priest ST. Discontinuity analysis for rock mechanics. London: Chapman & Hall, 1993 [chapter 10].